Numerical Simulation of the Bubble Cloud Dynamics in an Ultrasound Field

Kazuki Maeda* and Tim Colonius

Division of Engineering and Applied Science, California Institute of Technology

1200 E California Blvd, Pasadena, CA 91125, USA

Abstract

We use a coupled Eulerian-Lagrangian method to simulate the dynamics of a spherical bubble cloud with various void fractions excited by high-amplitude ultrasound pulses. We consider two cases: a single cycle of a sinusoidal waveform whose wavelength is large compared to the cloud diameter, and multiple cycles with a short wavelength. For the long wavelength, bubble cloud dynamics are nearly spherically symmetric. Bubbles near the periphery grow more than the those close to the center, and the collapse of bubbles propagates inward from the periphery of the cloud. The structure and the dynamics of the cloud are scaled with the cloud interaction parameter introduce by d'Agostino and Brennen. It is shown that polydispersity does not significantly alter the cloud dynamics. In the short wavelength case, the clouds develop an anisotropic structure in the direction of the incident wave propagation. Over a wide range of the void fraction, the distal side of the cloud is shielded from the incident wave and bubbles grow less. As characterized by the center of volume of the cloud, the anisotropy is similar over the range of volume fractions considered. The results of the study can be used to characterize the acoustic cavitation in ultrasound therapies.

Keywords: cloud cavitation; numerical simulation; Eulerian-Lagrangian method

Introduction

The dynamics of bubble clouds nucleated by ultrasound are important for successful outcomes of ultrasound therapy, including high-intensity focused ultrasound (HIFU) and lithotripsy. Bubbles can collapse violently to cause tissue injuries as well as to scatter and absorb incident ultrasound waves and reduce the energy focused on the target [1-3]. Due to the fast, unsteady nature of the bubble cloud dynamics of the bubble clouds, accurate, quantitative experimental measurements are limited, and therefore modeling and numerical simulations have been essential tools for understanding the physical mechanisms at play. Many previous studies have focused on the dynamics of monodisperse, spherical bubble clouds in an otherwise incompressible liquid so that the wavelength of the pressure excitation is much larger than the size of the cloud. D'Agostino and Brennen [4] used a volume averaging approach to analyzed the linearized dynamics of spherical bubble clouds under weak pressure excitation and found that the cloud interaction parameter, $B = \beta R_C^2/R_b^2$, dictates the effect of inter-bubble interaction on the resulting dynamics of the cloud, where β is the void fraction, R_C and R_b are the radii of the cloud and the bubbles, respectively. Wang and Brennen [5] extended the study to the nonlinear regime, observing strong collapses involving bubbly shock waves that propagate inward from the periphery of the cloud. Matsumoto and Yoshizawa used a similar approach to quantify amplifications of the collapse when excited by HIFU waves with a resonant frequency of the cloud, and discussed applications of the collapse energy to ablate a target in medical applications [6]. More recently, Ma *et al* used an Eulerian-Lagrangian approach to investigate the dynamics of bubble clouds near a rigid wall excited by pressure waves [7].

In practical applications of HIFU and lithotripsy, the scale separation invoked above does not necessary hold; bubble clouds with a size of $O(1)$ mm have been observed *in vitro* during the passage of a strong ultrasound wave with a wavelength of $O(1)$ mm [8]. In order to gain insights into such clouds, we simulate the dynamics of spherical bubble clouds with a radius of 2.5 mm containing bubbles with a mean initial radius of 10 um excited by an ultrasound wave with an amplitude of 1 MPa. The simulation uses a coupled Eulerian-Lagrangian method for bubbly-liquid that can capture the dynamics of individual spherical bubbles and the fine structure of the pressure field. The numerical method and its validation have been described elsewhere [9]. We use the following two kinds of ultrasound wave: 1 cycle of a sinusoidal wave with a wavelength of 30 mm, and 10 cycles of a sinusoidal wave with a wavelength of 5 mm. These cases are chosen to explore the differing bubble cloud dynamics when the wavelength is either long or short compared to the cloud size. For each wave, we conduct a parametric study varying the volume fraction of bubbles, and thus cloud interaction parameter. In the long wavelength case, we qualitatively reproduce the results of the aforementioned studies invoking the scale separation. We show that the dynamics of the clouds are not significantly altered by the

*Corresponding Author, Kazuki Maeda: maeda@caltech.edu

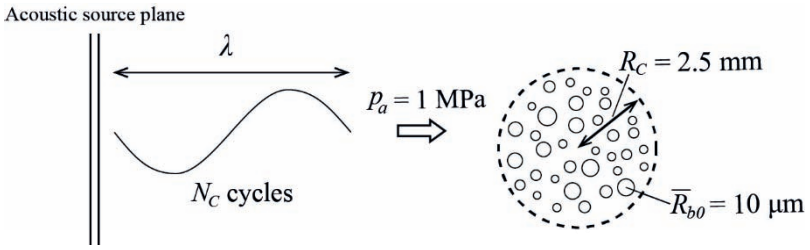

Figure 1. Schematic of the problem.

	σ	N_C	λ / R_C
Case 1	0	1	12
Case 2	0.7	1	12
Case 3	0	10	2

Table 1. Parameters used in the simulation cases

polydispersity of the bubbles. For the short wavelength case, we observe an anisotropic structure in the cloud during the passage of the wave, in that the proximal bubbles grow to larger radius than those in the distal side, within a wide range of the parameters of the cloud. This anisotropy is the result of a shielding of the distal bubbles from the incident wave. We discovered that the anisotropy is well characterized by the center of volume in the clouds.

Problem statement

Fig. 1 shows a schematic of the problem. We send N_C cycles of a planer, sinusoidal pressure wave with an amplitude of 1 MPa and a wavelength of λ mm from an acoustic source plane to a spherical bubble cloud with a radius of 2.5 mm. Bubbles are randomly seeded in the cloud in the initial condition. The initial radii of the bubbles, R_{b0}, are selected from a log normal distribution that follows $\ln(R_{b0}/\bar{R}_{b0}) \sim N(0, \sigma^2)$, where $\bar{R}_{b0}$ is the reference value of the initial radius: $\bar{R}_{b0}$ = 10 um. We characterize the bubble cloud by using the cloud interaction parameter defined as $B = \beta R_C^2/R_b^2 \sim N_b \bar{R}_b/R_C$, where N_b is the total number of the bubbles in the cloud. This expression of B is useful since it is independent of the polydispersity. The combinations of N, λ and σ addressed in the simulation are summarized in table 1. In all the cases, we vary N_b to realize the four distinct values of B: B = [0.625, 1.25, 2.5, 5]. Note that in the monodisperse case, B is a linear function of the void fraction. For each set of parameters, we run five independent simulations with randomized bubble positions in order to assess the variability with respect to the distribution of bubbles.

Numerical setup

We simulate the dynamics of bubbly-mixture using an Eulerian-Lagrangian method [9]. We discretize the governing equations on an axi-symmetric grid and integrate it using a finite volume, fifth-order WENO scheme. The incident pressure wave propagates in the positive axial (+x) direction. The grid size is uniform with a radial and axial grid spacing of 100 μm in the wave-cloud interaction region. The bubbles are modeled as sub-grid-scale spherical cavities that experience volumetric oscillations excited by pressure fluctuations in the surrounding liquid. The radial evolutions of each bubble is found by solving the Keller-Miksis equation. Heat and mass transfer across the bubble-water surface are accounted for using a reduced order model. Bubble-scattered pressure waves are resolved on the grid. The incident pressure wave is generated with a source-term approach [10].

Results and discussion: long wavelength cases

In this section we discuss the results of the long wavelength cases (case 1 and 2). Fig. 1a and b show the evolutions of the void fraction for several different values of B for the monodisperse (case 1) and polydisperse (case 2) clouds, respectively. In all clouds, after the passage of the incident wave, the void fraction steadily grows to reach its maximum

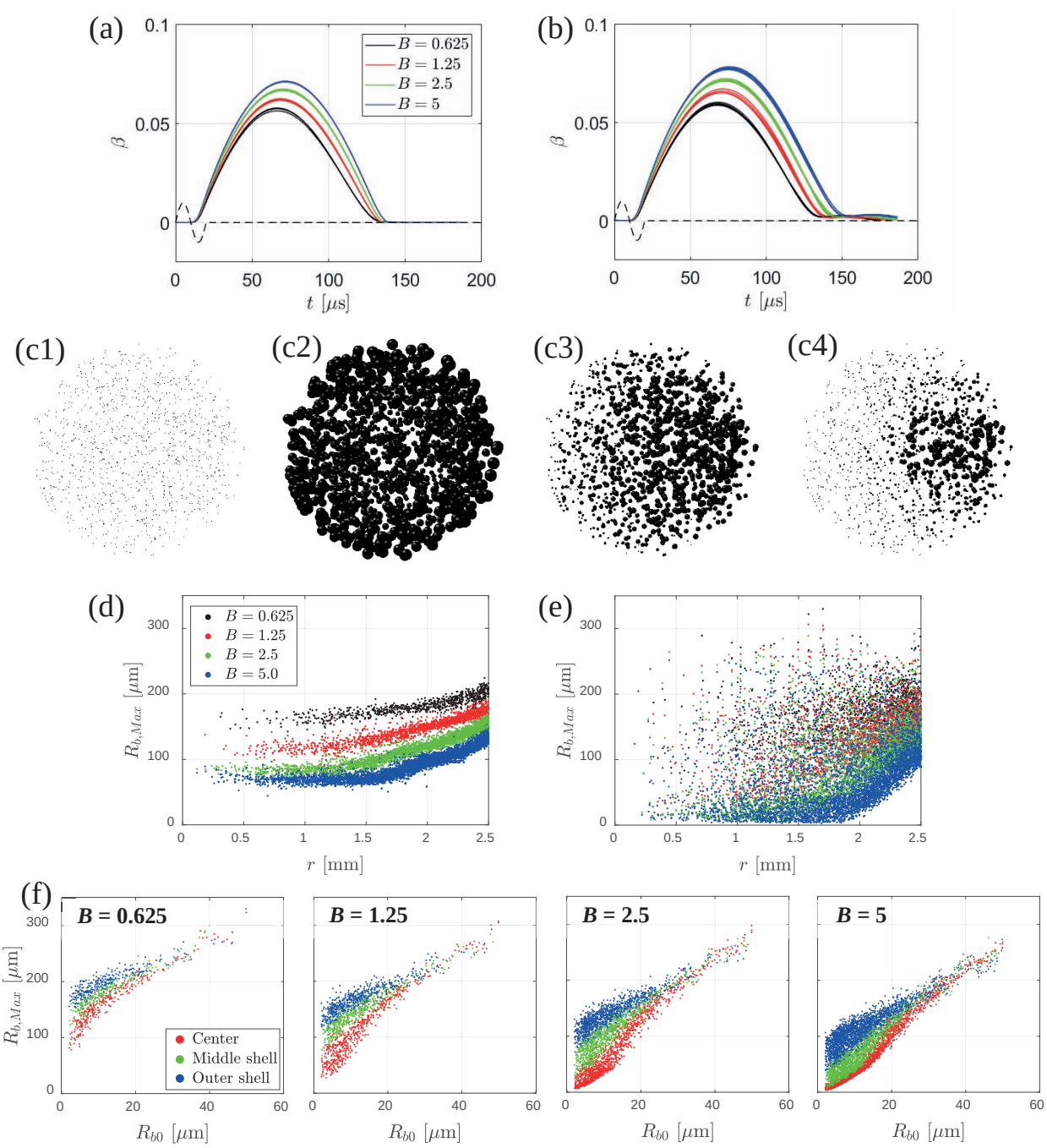

Figure2. (a,b) Evolution of the void fraction of the clouds. The dotted lines indicate the (scaled) incident wave pressure at the cloud center without bubble. For each value of *B*, all 5 runs with different randomized bubble positions are shown. (c1-4) Images of the initially monodisperse bubble cloud with $B = 5$ at t = 0, 76, 138, and 145 us. (d,e) Scatter plot of the maximum radii of each bubble over time and their radial coordinates. (f) Scatter plot of the maximum radii of the bubbles and their initial radii in the clouds of case2.

value around 0.05 – 0.08 at around t = 70 – 80 us, then collapses to zero at around t = 140 us. Slight rebounds are observed in the clouds in case2 after the collapse. The spread in the curves with the same value of *B* (same colors), resulting from the randomness of the coordinates of bubbles, are small in both cases. Interestingly, the results of case 1 and 2 do not show significant differences, suggesting that the effect of polydispersity is small. Fig. 1 c1-c4 show images of a representative cloud in case1 with $B = 5$ at the initial condition (c1), at its maximum void fraction (c2), and during the collapse (c3 and 4). The structures of the clouds possess nearly spherical symmetry, as bubbles

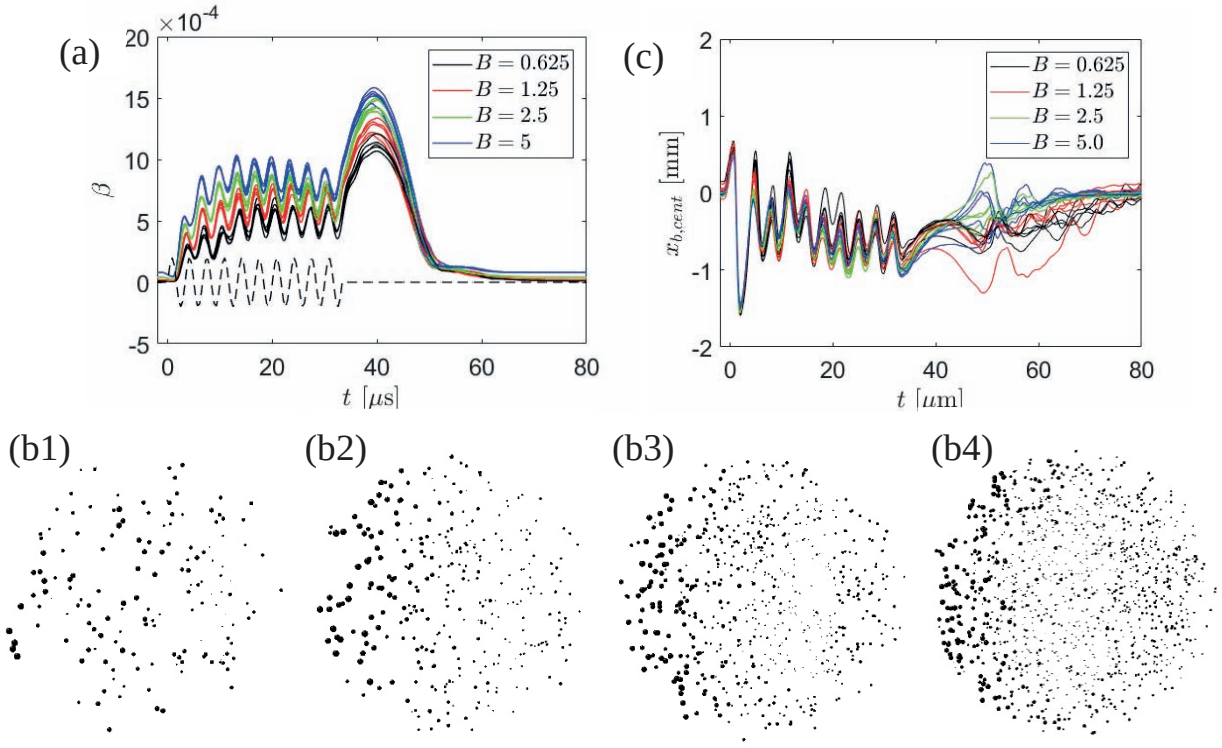

Figure 4. (a) Evolutions of the void fraction of the clouds. (b1-4). Images of bubble clouds with distinct values of *B: B* = 0.625, 1.25, 2.5 and 5, at *t* = 33 us. (c) Evolution of the volumetric center of the clouds.

experience uniform back-ground pressure during the passage of the incident wave due to its long wavelength. At its maximum void fraction, bubbles near the periphery of the cloud are larger than those near the center (c2). This can be explained by a shielding of the inner bubbles by the outermost layer; the outer bubbles scatter/absorb the acoustic energy of the incident wave to mitigate its penetration into the center. During the collapse, it is observed that the bubbles near the periphery collapse earlier, followed by the inner bubbles. This inward propagation of the collapse corresponds to the bubble cloud collapse involving bubbly-shockwave observed in the previous simulation [9] and experimental study [11]. The geometric center of the collapse is slightly offset to the right from the cloud center of the cloud in the present result. This offset can be explained by the slight delay in the arrival of the incident wave at the right side of the cloud due to the finite wavelength and the sound speed that were not considered in the previous studies.

In order to quantify the anisotropy in the growth of bubbles in the cloud, in fig. 2d and e we plot the maximum radius of the bubbles as a function of their radial coordinates (distance from the origin) for each value of *B*, for the monodisperse and polydisperse cases, respectively. In the monodisperse case (fig. 2d), the maximum radius has a clear monotonic, positive correlation with the radial coordinate. The slope of the correlation is increased with *B*, though the values of the radius tend to decrease with *B*. This results suggest that with increasing the inter-bubble interaction, the bubble growth is suppressed and anisotropy in the bubble growth is enhanced, as discussed in the aforementioned studies [4,5]. In the polydisperse case (fig. 2e), we do not observe clear correlations except for $B = 5$ indicated by a blue scattered points, due to higher dispersions in the bubble radius. For a better analysis of the polydisperse clouds, in fig. 2f we scatter the data points of the maximum radius of each bubble as a function of its initial radius separately for distinct values of *B*, with distinct colors based on bubble's radial coordinate: $r \in [0, 1.74]$ (center); [1.74, 2.18] (middle shell); [2.18, 2.5] mm (outer shell). Note that these three regions have approximately the same volume. The results show that for each value of *B*, the bubbles attain the largest radii in the outer shell, followed by the middle shell. The maximum radius tends to decrease by increasing *B*. Thus, it is indicated that the correlations observed in the monodisperse clouds hold true in the polydisperse case.

Results and discussion: short wavelength case

In this section we discuss results of the short wavelength case (case 3). We note that a single simulation of a similar cloud B = 2.5 and a weak polydispersity was reported in our previous study [9]. Fig. 4a shows the evolution of the void fraction of the clouds. For all the clouds, during the passage of the wave around until t = 35 us, the void fraction oscillates around at 0.5 - 1.0×10^{-3}. After the passage of the wave, it grows to reach its maximum value of 1.0 - 1.6×10^{-3} around at t = 40 us, then decays to reach zero around at t = 60 us. Variability due to the random positions of the bubbles is small. Fig. 4b1-4 show images taken during the passage of the incident wave with distinct values of B at t = 33 us. In all cases, we observe anisotropic structures in the cloud, whereby that the proximal side of bubbles grow more than those in the distal side. In the previous study, it was discussed that the anisotropy was the result of a shielding of the distal bubbles by the proximal ones. In order to quantify the anisotropy, we define the center of volume of the cloud:

$$x_{b,cent} = \frac{\sum_{cloud} \frac{4\pi}{3} R_b^3 x_b}{\sum_{cloud} \frac{4\pi}{3} R_b^3},$$

where x_b is the axial coordinate of each bubble. Fig. 4c plots the result. Interestingly, during the passage of the wave, until around t = 35 us, the evolution of $x_{b,cent}$ is similar for all simulations and oscillates between 0 and -1 mm. After the passage of the wave, $x_{b,cent}$ decays to zero with high variability. This result suggests that the structural anisotropy is always excited in the cloud during the passage of the wave and it is characterized by $x_{b,cent}$, regardless of the initial condition of the cloud within the range of parameters addressed in the present study.

Conclusion

We simulated the dynamics of bubble clouds with various cloud interaction parameters. With a single wavelength much larger than the cloud, the resulting cloud dynamics are nearly spherically symmetric, involve shielding by outer bubbles, and coherent cloud collapse propagating from the periphery toward the center. The results were scaled with the cloud interaction parameter, as formulated in the long wavelength limit [5]. We showed that the initial polydispersity of bubbles does not significantly alter the resulting dynamics of the clouds. With 10 cycles of a wave with a wavelength shorter than the cloud, an anisotropic structure is observed. The proximal bubbles in the cloud shield the distal bubbles. As characterized by the center of volume of the cloud, the anisotropy was similar for all cases simulated. The results of the study could be used to further understand and characterize the dynamics of cavitation bubble clouds formed during HIFU therapy and lithotripsy. Future work includes assessment of the far-field acoustics and the effect of polydispersity on the cloud dynamics in the short wavelength case as well as experimental validation.

Acknowledgement

K.M would like to acknowledge the Funai Foundation for Information Technology, for the Overseas Scholarship. This work was supported by the National Institutes of Health under grant P01-DK043881 and in part by the Office of Naval Research under grant N00014-17-1-2676. The simulations presented here utilized the Extreme Science and Engineering Discovery Environment, which is supported by the National Science Foundation grant number CTS120005.

References

[1] Pishchalnikov, Y.A., Sapozhnikov O.A, Bailey, M.R., Williams, J.C., Cleveland, R.O., Colonius, T., Crum, L.A., Evan, A.P., McAteer, J.A. (2004). *Cavitation Bubble Cluster Activity in the Breakage of Kidney Stones by Lithotripter Shockwaves*. Journal of Endourology. 17(7).

[2] Ikeda, I., Yoshizawa, S., Tosaki, M., Allen, J.S., Takagi, S., Ohta, N., Kitamura, T., Matsumoto, Y., (2006). *Cloud cavitation control for lithotripsy using high intensity focused ultrasound*. Ultrasound in medicine & biology. 32(9).

[3] Bailey, M.R., McAteer, J.A., Pishchalnikov, Y.A., Hamilton, M.F., and Colonius, T. (2006). *Progress in Lithotoripsy Research*. Acoustics Today. 3, 18-29.

[4] D'Agostino, L. and Brennen, C.E. (1989). *Linearized dynamics of spherical bubble clouds*. Journal of Fluid Mechanics. 199, 155-176.

[5] Wang, Y-C. and Brennen, C.E. (1999). *Numerical Computation of Shock Waves in a Spherical Cloud of Cavitation Bubbles*. Journal of Fluids Engineering. ASME Journal of Fluid Engineering. 121(4).

[6] Matsumoto, Y. and Yoshizawa, S. (2005). *Behaviour of a bubble cluster in an ultrasound field*. International Journal for Numerical Methods in Fluids. 47, 591-601.
[7] Ma, J., Hsial, C-T., Chahine, G.L. (2018). *Numerical study of acoustically driven bubble cloud dynamics near a rigid wall*. Ultrasonics Sonochemistry. 40, 944-954.
[8] Maeda, K., Kreider, W., Maxwell, D., Cunitz, B., Colonius, T., Bailey, M. (2015). *Modeling and experimental analysis of acoustic cavitation bubbles for Burst Wave Lithotripsy*. Journal of Physics: Conference Series. 656(1).
[9] Maeda, K. and Colonius, T. (2017). *Eulerian-Lagrangian method for simulation of cloud cavitation*. arXiv preprint arXiv:1712.00670.
[10] Maeda, K. and Colonius, T. (2017). *A source term approach for generation of one-way acoustic waves in the Euler and Navier-Stokes equations*. Wave Motion. 75, 36-49.
[11] Arora, M., Ohl, C.D., Lohse, D. (2007). *Effect of nuclei concentration on cavitation cluster dynamics*. The Journal of the Acoustical Society of America. 121, 3242.